Solution Structure of Calcium-Bound Rat S100B(ββ) As Determined by Nuclear Magnetic Resonance Spectroscopy † , ‡

ARTICLE *in* BIOCHEMISTRY · MARCH 1998

Impact Factor: 3.02 · DOI: 10.1021/bi972635p · Source: PubMed

4 AUTHORS, INCLUDING:

Alexander C Drohat
University of Maryland, Baltimore
48 PUBLICATIONS **1,897** CITATIONS
SEE PROFILE

Richard R Rustandi
Merck
47 PUBLICATIONS **1,332** CITATIONS
SEE PROFILE

David Joseph Weber
University of Maryland, Baltimore
126 PUBLICATIONS **3,830** CITATIONS
SEE PROFILE

Solution Structure of Calcium-Bound Rat S100B($\beta\beta$) As Determined by Nuclear Magnetic Resonance Spectroscopy[†,‡]

Alexander C. Drohat, Donna M. Baldisseri, Richard R. Rustandi, and David J. Weber*

Department of Biochemistry and Molecular Biology, University of Maryland School of Medicine, 108 North Greene Street, Baltimore, Maryland 21201

Received October 23, 1997; Revised Manuscript Received December 15, 1997

ABSTRACT: The three-dimensional structure of Ca^{2+}-bound rat S100B($\beta\beta$) has been determined using data from a series of two-dimensional (2D), three-dimensional (3D), and four-dimensional (4D) nuclear magnetic resonance (NMR) experiments. Each S100β subunit (91 residues) contains four helixes (helix 1, E2−R20; helix 2, K29−N38; helix 3, Q50−D61; and helix 4, F70−A83) and one antiparallel β-sheet (strand 1, K26−K28; and strand 2, E67−D69) which brings the normal and pseudo EF-hands together. As found previously for rat apo-S100B($\beta\beta$) [Drohat, A. C., et al. (1996) *Biochemistry 35*, 11577−11588], helixes 1, 1′, 4, and 4′ associate to form an X-type four-helix bundle at the symmetric dimer interface. Additionally, Ca^{2+} binding does not significantly change the interhelical angle of helixes 1 and 2 in the pseudo EF-hand (apo, $\Omega_{1-2} = 132 \pm 4°$; and Ca^{2+}-bound, $\Omega_{1-2} = 137 \pm 5°$). However, the interhelical angle of helixes 3 and 4 in the normal EF-hand ($\Omega_{3-4} = 106 \pm 4°$) changed significantly upon the addition of Ca^{2+} ($\Delta\Omega_{3-4} = 112 \pm 5°$) and is similar to that of the Ca^{2+}-bound EF-hands in calbindin D_{9K}, calmodulin, and troponin ($84° \leq \Omega \leq 128°$). Further, the four helixes within each S100β subunit form a splayed-type four-helix bundle (four perpendicular helixes) as observed in Ca^{2+}-bound calbindin D_{9K}. The large Ca^{2+}-dependent conformational change involving helix 3 exposes a cleft, defined by residues in the hinge region, the C-terminal loop, and helix 3, which is absent in the apo structure. This surface on Ca^{2+}-bound S100B($\beta\beta$) is likely important for target protein binding.

S100B is a highly conserved Ca^{2+}-binding protein that is expressed in a wide variety of tissues and cell lines, including malignant tumors (*1*−*5*). The gene for S100B is mapped to the Down's syndrome region of human chromosome 21 (bands 21q22.2 and 22.3), and levels of S100B are significantly increased in activated astrocytes surrounding neuritic plaques for patients with Alzheimer's disease (*6*, *7*). S100B transgenic mice are found to undergo astrocytosis and neurite proliferation, suggesting that an excess of S100B may be relevant to the neuropathology associated with these diseases (*8*). While the precise mechanisms for intra- and extracellular functions of S100B are not well understood, it is known that processes such as neurite extension, Ca^{2+} flux, cell growth, apoptosis, energy metabolism, and protein phosphorylation are all modulated in some manner by S100B (*1*−*5*).

The mechanism by which S100B functions is thought to depend upon tightly regulated intra- and extracellular Ca^{2+} ion concentrations (*9*). Characteristic of all S100 proteins, the first helix−loop−helix Ca^{2+}-binding domain of each S100β[1] subunit (S18−E31) has two more amino acid residues than typical EF-hand domains (14 vs 12 residues). Furthermore, several of the Ca^{2+}-liganding residues of the S100-hand (or pseudo EF-hand) do not conform to those of the EF-hand consensus sequence (*10*−*12*). Accordingly, the pseudo EF-hand binds Ca^{2+} with low affinity ($K_D = 200-500\ \mu M$) (*13*), whereas the second Ca^{2+}-binding domain (D61−E72) contains the consensus EF-hand sequence and binds Ca^{2+} with relatively high affinity ($K_D = 20-50\ \mu M$) (*2*, *10*−*13*).

The general model for S100−target protein interactions is similar to that of other Ca^{2+}-binding proteins such as calmodulin and troponin C. As observed for these proteins, Ca^{2+} promotes a conformational change that is required for the binding of S100B to a variety of target proteins (*2*−*5*,

[†] This work was supported in part by a National Institutes of Health grant (R29GM5207 to D.J.W.), an American Cancer Society grant (JFRA-641 to D.J.W.), and by SRIS and DRIF funding from The University of Maryland School of Medicine and the State of Maryland (to D.J.W.). This study made use of a 600 MHz NMR spectrometer in the UMAB NMR facility which was purchased with funds from the University of Maryland and the NIH shared instrumentation grant program (S10RR10441 to D.J.W.).

[‡] Coordinates for the 20 structures of Ca^{2+}-bound rat S100B($\beta\beta$) and the associated restraint files have been deposited at the Brookhaven Protein Data Bank under the file name 1QLK.

* To whom correspondence should be addressed. Phone: (410) 706-4354. Fax: (410) 706-0458. E-mail: weber@noe.ab.umd.edu.

[1] Abbreviations: BCA, bicinchoninic acid; βME, β-mercaptoethanol; DGSA, distance geometry-simulated annealing; DTT, dithiothreitol; HOHAHA, homonuclear Hartmann−Hahn; HMQC, heteronuclear multiple-quantum coherence; HSQC, heteronuclear single-quantum coherence; MARCKS, myristoylated alanine-rich kinase C substrate protein; NMR, nuclear magnetic resonance; NOE, nuclear Overhauser effect; NOESY, NOE spectroscopy; PKC, protein kinase C; rmsd, root-mean-square difference; ROESY, rotating frame Overhauser effect spectroscopy; S100β, subunit of dimeric S100B; S100B($\beta\beta$), dimeric S100B with noncovalent interactions at the dimer interface; S100B-(β-β), dimeric S100B with disulfide bonds at the dimer interface; TPPI, time-proportional phase incrementation; Tris-HCl, tris(hydroxymethyl)-aminomethane hydrochloride; TSP, sodium 3-(trimethylsilyl)propionate-2,2,3,3-d_4.

S0006-2960(97)02635-4 CCC: $15.00
Published on Web 02/12/1998

14, *15*). For example, the Ca^{2+}-dependent binding of reduced S100B($\beta\beta$) to microtubules (*16*), GFAP (*17*), and p53 (*18*) prevents oligomerization for each of these proteins. Furthermore, Ca^{2+}-bound S100B($\beta\beta$) inhibits the PKC-dependent phosphorylation of τ-protein (*19*), GAP-43 (*20*, *21*), MARCKS (*22*), and p53 (*18*, *23*) by binding to the phosphorylation site of these PKC substrates. Interestingly, loop 2 (the hinge region) and the C terminus of S100B($\beta\beta$) are thought to directly interact with target proteins since these regions of S100 proteins lack sequence homology and are proximal in the solution structure of rat apo-S100B($\beta\beta$) (*2*, *14*).

To further characterize S100B($\beta\beta$), its three-dimensional structure was determined in the presence of Ca^{2+} using a series of two-dimensional (2D), three-dimensional (3D), and four-dimensional (4D) NMR spectroscopy experiments. As for the apoprotein, Ca^{2+}-bound S100B($\beta\beta$) was found to be highly structured with the two EF-hands brought into close proximity with a short two-stranded antiparallel β-sheet (*12*, *14*). In addition, the X-type four-helix bundle which comprises the dimer interface of Ca^{2+}-bound S100B($\beta\beta$) is similar to that found in apo-S100B($\beta\beta$) (*14*). However, helixes 3 and 4 in apo-S100B($\beta\beta$) have an interhelical angle which is significantly different (>110°) from that in Ca^{2+}-bound S100B($\beta\beta$). This large conformational change upon the addition of Ca^{2+} readily explains the significant changes observed in chemical shift and amide exchange rates, and most likely accounts for the Ca^{2+} dependence of target protein binding observed for S100B($\beta\beta$).

MATERIALS AND METHODS

Materials. All chemical reagents were ACS grade or higher and purchased from Sigma unless otherwise indicated. Buffers were passed through Chelex-100 resin (BioRad) to remove trace metals. Perdeuterated Tris, d_{11}-Tris (1 M solution in D_2O, >98.7 at. % deuterium), was purchased from C/D/N Isotopes, Inc. (Vandreuil, Quebec, Canada), and D_2O (100.0 at. % deuterium, low in paramagnetic impurities) was purchased from Aldrich Chemical Co. (Milwaukee, WI). $^{15}NH_4Cl$ (>99%) and ^{13}C-labeled glucose were purchased from Cambridge Isotope Laboratories (Woburn, MA).

S100B($\beta\beta$) Sample Preparation. Recombinant S100B($\beta\beta$) was overexpressed in *Escherichia coli* strain HMS174(DE3) transformed with an expression plasmid containing the rat S100β gene. Unlabeled, ^{15}N-labeled, and ^{13}C,^{15}N-labeled S100B($\beta\beta$) were prepared and purified (>99%) under reducing conditions using procedures similar to those described previously (*12*, *14*, *24*), except that 0.5 mM DTT (Gibco BRL) was used as a reducing agent throughout the preparation instead of β-mercaptoethanol. The reported subunit concentrations of S100B($\beta\beta$) were determined using a BCA protein assay with an S100B($\beta\beta$) standard with a known subunit concentration as previously described (*14*, *24*).

Unless otherwise stated, solution conditions for the NMR samples were 3 mM (subunit concentration) S100B($\beta\beta$), 6.1 mM $CaCl_2$, 0.34 mM NaN_3, 5 mM DTT, 5−10% D_2O, 6−10 mM d_{11}-Tris-HCl (pH 6.5), and sufficient NaCl (17−20 mM) to give an ionic strength equal to 25 mM at 37 °C. An additional NMR sample was used in experiments designed to distinguish intra- and intermolecular NOEs at the dimer interface of S100B($\beta\beta$). This sample contained a 50:50 mixture of unlabeled and ^{13}C,^{15}N-labeled S100B($\beta\beta$) (1.5 mM subunit concentration for each) with all other conditions the same.

Table 1: NMR-Derived Restraints and Statistics of NMR Structures[a]

	⟨20⟩	best
rmsds from exptl distance restraints (Å)[b]		
all (2158)	0.030 ± 0.004	0.026
intraresidue (372)	0.025 ± 0.009	0.024
sequential ($\|i-j\|=1$) (556)	0.028 ± 0.007	0.026
medium-range ($1<\|i-j\|\le 5$) (636)	0.014 ± 0.008	0.011
long-range ($\|i-j\|>5$) (258)	0.038 ± 0.009	0.038
intermolecular (138)	0.027 ± 0.018	0.026
intra- and/or intermolecular (26)	0.019 ± 0.027	0.049
hydrogen bonds (152)	0.024 ± 0.014	0.026
calcium ligand (20)	0.142 ± 0.051	0.099
rmsds from exptl dihedral restraints (deg) (122)[b]	0.218 ± 0.140	0.203
rmsds from exptl ^{13}C chemical shifts		
$^{13}C\alpha$ (ppm)	1.239 ± 0.056	1.141
$^{13}C\beta$ (ppm)	1.034 ± 0.040	0.993
rmsds from idealized covalent geometry		
bonds (Å)	0.003 ± 0.001	0.003
angles (deg)	0.361 ± 0.029	0.340
impropers (deg)	0.341 ± 0.037	0.298
Lennard-Jones potential energy (kcal/mol)[c]	−777 ± 88	−779
% of residues in the most favorable region of the Ramachandran plot[d]	87.7 ± 1.7	91.9
bad contacts per 100 residues[d]	8.2 ± 3.4	10.9
H-bond energy SD[d]	0.79 ± 0.06	0.83
overall dihedral *G* factor[d]	0.27 ± 0.05	0.30
rmsds to the mean structure (Å)[e]		
backbone in pseudo EF-hand (2−38)	1.05 ± 0.22	0.57
backbone in typical EF-hand (50−83)	1.02 ± 0.18	0.77
all ordered backbone residues (1−88)	1.27 ± 0.19	0.86
all ordered heavy atoms (1−88)	1.92 ± 0.17	1.63

[a] ⟨20⟩ are the ensemble of 20 simulated annealing (SA) structures. The best was chosen on the basis of its quality as measured by the statistics given in this table and as discussed in the text. For ⟨20⟩, values shown are mean ± standard deviation. The final force constants of the target functions employed in the SA refinement were as follows: 1000 kcal mol^{-1} $Å^{-2}$ for bond lengths, 500 kcal mol^{-1} rad^{-2} for angles and improper torsions, 4 kcal mol^{-1} $Å^{-4}$ for the quartic van der Waals (vdw) repulsion term (hard sphere effective vdw radii set to 0.80 times their value in the CHARMM parameters), 30 kcal mol^{-1} $Å^{-2}$ for experimental distance restraints, 200 kcal mol^{-1} rad^{-2} for (ϕ) dihedral angle restraints, 100 kcal mol^{-1} $Å^{-2}$ for noncrystallographic symmetry, 1 kcal mol^{-1} $Å^{-2}$ for distance symmetry restraints, 0.5 kcal mol^{-1} ppm^{-2} for ^{13}C shift restraints, and 1.0 for the conformational data base potential. [b] None of the structures exhibited a distance violation of >0.5 Å or a dihedral angle violation of >5°. [c] The Lennard-Jones van der Waals energy was calculated using the CHARMM parameters and was not employed in any stage of structure determination. [d] For parameters calculated using PROCHECK (*67*), good quality structures are expected to exhibit less than 10 bad contacts per 100 residues, an H-bond SD of 0.5−1.0, and a dihedral *G* factor of greater than −0.5. [e] Backbone calculations included Cα, N, and C′ atoms. Ordered residues included 1−88 since no long-range NOEs were observed for residues 89−91.

NMR Spectroscopy. The NMR experiments necessary for the structure determination of Ca^{2+}-bound S100B($\beta\beta$) are given in Table 1 of the Supporting Information. Heteronuclear NMR spectra were collected at 37 °C with a Bruker DMX600 NMR spectrometer (600.13 MHz for protons) equipped with four frequency channels and a triple-resonance three-axis gradient probe. Unless otherwise stated, a 1 s relaxation delay was used, and quadrature detection in the indirect dimensions was obtained with States−TPPI phase

cycling (*25*). Initial delays in the indirect dimensions were set to give zero- and first-order phase corrections of 90 and −180°, respectively (*26*). Data were processed on Silicon Graphics workstations using nmrPipe (*27*). Time domain data in the indirect dimensions were extended by no more than 50% using standard linear prediction routines (*28*), except for data in constant time domains which were extended 2-fold using mirror-image linear prediction (*29*). Proton chemical shifts are reported with respect to the H_2O or HDO signal taken as 4.658 ppm relative to external TSP (0.0 ppm) at 37 °C. The ^{13}C and ^{15}N chemical shifts were indirectly referenced using the following ratios of the zero-point frequencies at 37 °C: 0.101 329 05 for ^{15}N to ^{1}H and 0.251 449 53 for ^{13}C to ^{1}H (*30*−*32*).

Unlabeled S100B($\beta\beta$) in H_2O (10% D_2O) was used to record the 2D NOESY (*33*), ROESY (*34*), and TOCSY (*35*) experiments. Uniformly ^{15}N-labeled S100B($\beta\beta$) was used to collect the 2D $^{1}H-^{15}N$ fast HSQC (*36*), the 3D ^{15}N-edited NOESY-HSQC (*37*), the 3D ^{15}N-edited clean-HOHAHA-HSQC (*35*, *38*), and the 3D ^{15}N,^{15}N-edited HMQC-NOESY-HSQC (*39*) data. The ^{13}C,^{15}N-labeled sample was used to collect the 2D CT-HSQC data (*40*) with parameters optimized for detecting aromatic resonances as previously described (*41*) and the 3D ^{13}C-edited NOESY-HSQC (*42*), the 3D HNCACB (*43*), the 3D CBCA(CO)NH (*44*), the 4D ^{13}C,^{13}C-edited NOESY (*45*), and the sensitivity-enhanced 4D ^{13}C,^{15}N-edited NOESY-HSQC (*46*) data. The 3D ^{13}C-edited, ^{12}C-filtered HMQC-NOESY data(*14*, *47*) were collected on a sample containing equimolar unlabeled and ^{13}C,^{15}N-labeled S100B($\beta\beta$) (1.5 mM subunit concentration for each) to distinguish intra- and intermolecular NOEs. The fast HSQC detection scheme was incorporated in all ^{15}N-edited experiments to avoid water saturation (*36*), and pulsed field gradients were used as needed to purge undesired magnetization (*48*) and to provide sensitivity enhancement (*49*).

The sequence specific assignment of ^{1}H, ^{13}C, and ^{15}N resonances in Ca^{2+}-bound S100B($\beta\beta$) was determined using the 3D ^{15}N-edited clean-HOHAHA-HSQC, the 3D CBCA-(CO)NH and HNCACB, and the 3D HCCH-TOCSY data for through-bond correlations along the backbone and side chains. These assignments were confirmed by the observation of characteristic through-space correlations in the NOESY experiments, particularly in regions of regular secondary structure, as previously described (*50*). Assignment of aromatic residues was determined using the 2D NOESY, ROESY, and TOCSY, the 2D ^{13}C-edited CT-HSQC, and the 4D ^{13}C,^{13}C-edited NOESY experiments using standard techniques (*50*) as described for apo-S100B($\beta\beta$) (*14*). The ^{1}H, ^{13}C, and ^{15}N chemical shift values for Ca^{2+}-bound S100B($\beta\beta$) are similar in most cases to those of human S100B (*51*), and have been submitted to the BioMagResBank chemical shift data bank (accession number 4105) located at the University of Wisconsin at Madison. Hydrogen exchange of the backbone amide protons was measured by lyophilizing Ca^{2+}-bound S100B($\beta\beta$) from H_2O, dissolving it in D_2O, and immediately starting a series of fast ^{1}H,^{15}N-HSQC experiments with intervals of 0.25, 0.42, 0.50, 0.83, 1.5, 4.0, 8.0, 12, 18, and 24 h (*38*).

Structure Calculations. Inter-proton distance restraints derived from the NOESY and ROESY experiments were classified on the basis of peak intensity into categories with lower bounds of 1.8 Å and upper bounds of 2.7 (2.9 for NH), 3.3 (3.5 for NH), 4.2, 5.0, and 6.0 Å as previously described (*52*). Distances for degenerate or non-stereospecifically assigned protons were represented using an $(\sum r^{-6})^{-1/6}$ sum, as were distances for 26 intra- and intermolecular NOEs at the dimer interface which could not be classified strictly as intra- or intermolecular (*53*). Only structurally useful NOE restraints were included, and therefore, NOEs between geminal protons or between vicinal methylene protons were not used as restraints. Weak and very weak NOEs were used as restraints only when reciprocal NOE correlations with similar intensities were observed, and any NOE correlations suspected of having spin diffusion contributions to their intensity were confirmed by checking the sign and intensity of the same correlation in the 2D ROESY experiment. For the three residues (S1, K5, and H42) which exhibited two H_N resonances, distance restraints were employed only for those H_N NOEs that were observed with similar intensities at each of the two chemical shifts, as previously described (*14*). Backbone dihedral angle restraints (ϕ) of $-60 \pm 20°$ for α-helix and $-120 \pm 30°$ for β-strand were used only in regions of regular secondary structure as determined by hydrogen exchange rates, observation of characteristic NOE correlations, and secondary ^{1}H and ^{13}C chemical shifts (*54*). Backbone hydrogen bond restraints r_{NH-O} of 1.5−2.8 Å and r_{N-O} of 2.4−3.5 Å were used in the final stage of the structure determination for regions of regular secondary structure (*50*).

Initial structures of S100B($\beta\beta$) were determined using only unambiguous NOE correlations, and ambiguous NOEs were incorporated in an iterative manner as the quality of the structure improved using physical models and the calculated structures to resolve ambiguity. Structures were calculated with X-PLOR version 3.851 (*55*) using the standard protocols for substructure embedding and regularization, hybrid distance geometry-simulated annealing (DGSA) regularization and refinement, and simulated annealing (SA) refinement (*56*−*58*). The DGSA and SA routines employed noncrystallographic symmetry (NCS) and distance symmetry restraints with force constants of 100 and 1 kcal mol^{-1} $Å^{-2}$, respectively (*53*). The SA refinement included pseudopotentials for secondary $^{13}C\alpha$ and $^{13}C\beta$ chemical shifts (*59*) and a conformational data base potential (*60*, *61*). This refinement procedure yielded structures with no distance violations of >0.5 Å, no dihedral restraint violations of >5°, and low rmsds from the experimental restraints, and the values were of good quality on the basis of the measures listed in Table 1. These structures were used for an additional stage of refinement that included distance restraints from Ca^{2+} to protein ligands of 2.0−2.8 Å on the basis of the EF-hand model of Strynadka and James (*11*). The nomenclature for a consensus EF-hand identifies only six (*X*, *Y*, *Z*, $-X$, $-Y$, and $-Z$) of the possible seven sites of coordination for Ca^{2+} (*11*). For the consensus EF-hand of apo-S100B($\beta\beta$), we employed distance restraints from Ca^{2+} to the five consensus protein ligands (one of six consensus sites is a water), and added a restraint at the $-Z'$ position which, along with the $-Z$ position, generally exhibits bidentate coordination to the final glutamate (position 12) in the EF-hand (*11*). The pseudo EF-hand was modeled using 15 different sets of four ligands on the basis of the X-ray structure of the S100-hand in calbindin D_{9K} (*62*) and

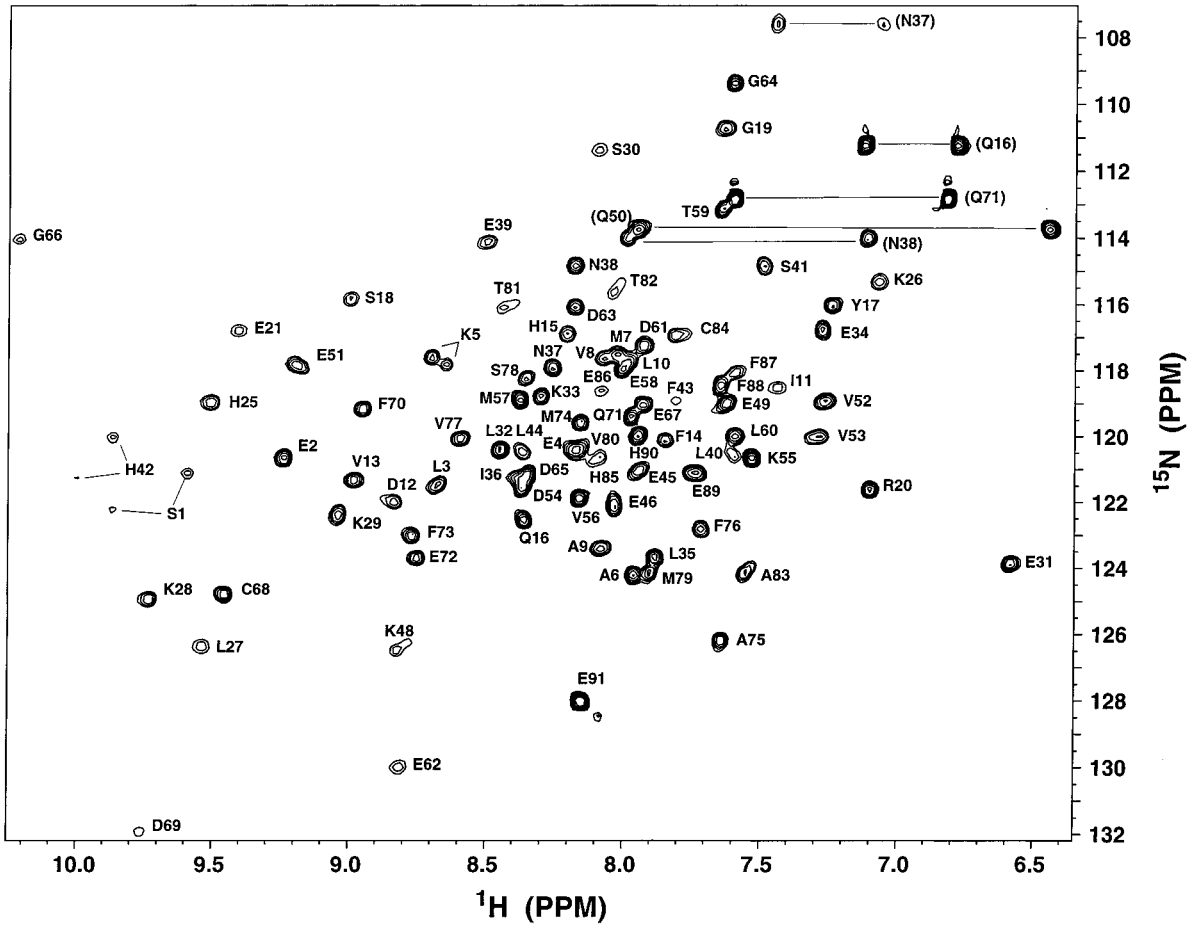

FIGURE 1: 2D ^{1}H−^{15}N HSQC of Ca^{2+}-bound S100B($\beta\beta$) with assignments. The correlations connected by horizontal lines correspond to glutamine and asparagine side chain NH_2 groups. Residues S1, K5, and H42 exhibit multiple correlations due to the presence or absence of an ***N***-formyl group at the amino terminus as previously described (*65*).

on the basis of lanthanide luminescence data (*15*). Color illustrations were produced with the computer graphics programs MIDAS and GRASP (*63*, *64*, *83*).

RESULTS AND DISCUSSION

Effects of Ca^{2+} on the NMR Spectra of Rat-S100B($\beta\beta$). Titrations of rat apo-S100B($\beta\beta$) with Ca^{2+} were monitored by 2D ^{1}H−^{15}N HSQC NMR experiments in an attempt to determine which residues of S100B($\beta\beta$) are most affected by Ca^{2+} binding. However, a large number of ^{1}H−^{15}N correlations (>80%) in the HSQC spectrum broadened below the baseline prior to saturation with Ca^{2+}. Correlations reappeared and narrowed as the titration proceeded above 1 equiv of Ca^{2+} per S100β subunit and stopped changing when Ca^{2+} concentrations exceeded 2 equiv per S100β subunit (Figure 1). Due to this exchange broadening, resonance assignments could not be made by merely following the ^{1}H−^{15}N correlations during Ca^{2+} titrations. Therefore, it was necessary to assign Ca^{2+}-bound S100B($\beta\beta$) a priori using a series of multidimensional heteronuclear NMR experiments (Table 1, Supporting Information) as previously found for human S100B (*51*).

The ^{1}H−^{15}N HSQC spectrum of Ca^{2+}-bound S100B($\beta\beta$) (Figure 1) exhibits significant changes in chemical shift compared to that of apo-S100B($\beta\beta$) for nearly all residues (*12*). Moreover, these changes occur throughout the protein (Figure 2). The residues significantly affected ($\Delta\delta^{1}H_N$ > 1 ppm, $\Delta\delta^{15}N$ > 2.0 ppm, $\Delta\delta^{1}H_{CH_3}$ > 0.5 ppm, $\Delta\delta^{1}H_\alpha$ > 0.5 ppm, and $\Delta\delta^{13}C_\alpha$ > 1 ppm) include K5, V8, I11, D12, and Q16 of helix 1; G19−D23 of loop 1; L27−K29 of the first β-strand; S30, E31, and K33−I36 of helix 2; H42, F43, E45, I47, and K48 of loop 2; Q50, D54, M57, L60, and D61 of helix 3; E62−G64 and G66 of loop 3; E67 and D69 of the second β-strand; F70, Q71, V77−M79, T81, and A83 of helix 4; and C84, H85, and F87−E89 of the C-terminal loop (Figure 2). The differences in chemical shift arise from either a direct interaction of these residues with Ca^{2+} and/or a Ca^{2+}-induced structural change in their immediate vicinity.

Amburgey et al. (*12*) previously found that 14 residues in helix 1 and the hinge region of rat apo-S100B($\beta\beta$) gave multiple ^{1}H−^{15}N correlations (S1, L3, E4, K5, A6, V8, L10, F14, S41, H42, F43, L44, E45, and E46). These multiple resonances arise from heterogeneous processing in *E. coli* which results in the presence of either a Ser, Met, or *N*-formyl-Met at the N terminus (*65*). However, in the presence of Ca^{2+}, we observed multiple resonances for only S1, K5, and H42 of recombinant S100B($\beta\beta$) (Figure 1). This result suggests that the amino terminus of the Ca^{2+}-bound S100B($\beta\beta$) is farther away from the hinge region than in apo-S100B($\beta\beta$) and/or it is less ordered in the presence of Ca^{2+}.

We have also found that many amide protons of Ca^{2+}-bound rat S100B($\beta\beta$) exchange more rapidly than those in apo-S100B($\beta\beta$) (Figure 3), and similar results were observed

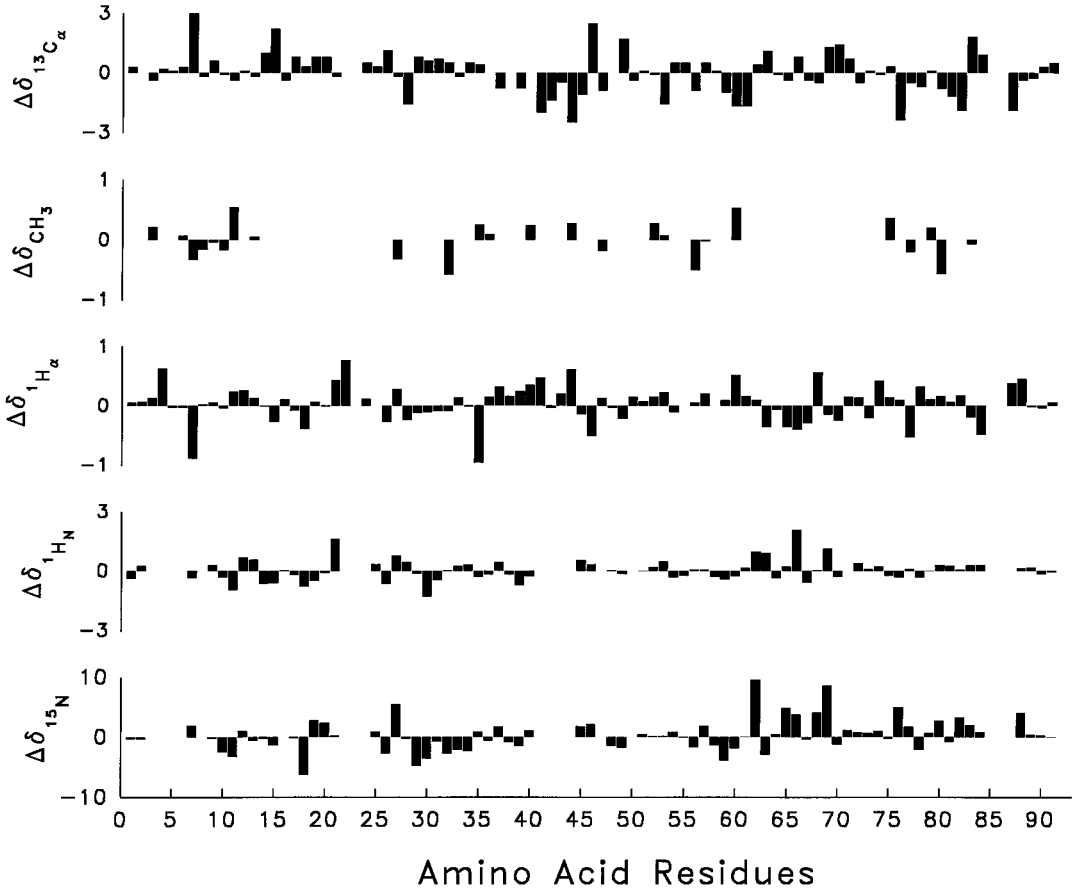

FIGURE 2: Change in chemical shift from apo- to Ca^{2+}-bound rat S100B($\beta\beta$) ($\Delta\delta^1H_N$, $\Delta\delta^1H_\alpha$, $\Delta\delta^1H_{CH_3}$, $\Delta\delta^{13}C_\alpha$, and $\Delta\delta^{15}N$) by amino acid residue.

for Ca^{2+}-bound human S100B (*51*). In particular, $^1H-^{15}N$ correlations of residues in helix 1 (L10), loop 1 (R20 and E21), helix 2 (S30, K33, and N37), the hinge region (E49), helix 3 (E51−V53, K55, and M57−D61), loop 3 (G64 and G66), helix 4 (Q71 and A83), and the C-terminal loop (F88 and E91) are absent after 0.25 h in D_2O for Ca^{2+}-bound S100B($\beta\beta$). On the other hand, $^1H-^{15}N$ correlations for these residues are observed more than 18 h after the addition of D_2O in apo-S100B($\beta\beta$) (*12*). Interestingly, many of these amide protons (10 of 26) are located in helix 3, and helix 3 is found to significantly change its orientation upon the addition of Ca^{2+}.

Analysis of the NOE Correlations. A significant amount of chemical shift degeneracy was encountered during the assignment of $^1H-^1H$ NOE correlations in Ca^{2+}-bound S100B($\beta\beta$). As for apo-S100B($\beta\beta$), these overlapping resonances are probably due to the presence of four α-helixes per S100β subunit and to the symmetric dimer interface (*12*, *14*). Therefore, the assignment of NOE correlations from 2D and 3D ^{15}N-edited NOESY data sets alone was very difficult, and 4D $^{13}C,^{15}N$-edited NOESY and $^{13}C,^{13}C$-edited NOESY experiments were used to resolve ambiguities in 2D and 3D data sets. As a result, over 60% of the long-range NOE correlations were assigned on the basis of unambiguous chemical shift values from the 4D data sets (Figure 4).

Throughout the NOE assignment process, it was also necessary to distinguish between intramolecular and intermolecular NOE correlations. This was done by comparing 3D ^{13}C-edited, ^{12}C-filtered HMQC-NOESY data collected with asymmetrically labeled S100B($\beta\beta$) to 4D $^{13}C,^{13}C$-edited NOESY data collected with a uniformly enriched sample. As found for apo-S100B($\beta\beta$) (*14*), the antiparallel alignment of helix 1 from one subunit with helix 1′ (the other subunit) was determined by the presence of several unambiguous intermolecular NOE correlations, including a strong NOE between methyl protons of L3 and V13 (Figure 4A,B). As a result, NOE correlations found in the 4D $^{13}C,^{15}N$-edited NOESY data such as the one observed between H_N of L3 and the methyl protons of V13 could be confidently assigned as intermolecular. Likewise, several intermolecular NOE correlations between protons from the N and C terminus of helix 4 were also assigned, indicating that helixes 4 and 4′ also align in an antiparallel manner at the dimer interface. These and other unambiguous intermolecular NOE assignments made it relatively straightforward to assign a large number of additional intermolecular NOE correlations at later stages in the refinement process when a detailed understanding of the structure emerged. In total, the dimer interface of Ca^{2+}-bound S100B($\beta\beta$) was defined by 138 intermolecular and 26 intra- and/or intermolecular NOEs involving residues in helix 1 (S1, E2, L3, K5, A6, M7, V8, A9, L10, I11, V13, and F14), helix 2 (L35 and I36), loop 2 (E39, L40, and F43), helix 4 (F70, Q71, M74, A75, F77, M79, T81, and T82), and loop 4 (C84 and F88).

Ca^{2+} Coordination. An examination of 20 refined structures of Ca^{2+}-bound S100B($\beta\beta$) that were calculated without Ca^{2+} distance restraints revealed that the overall geometry of the Ca^{2+}-binding loops (ϕ and ψ angles) and interhelical angles for the pseudo and typical EF-hands ($\Omega_{1-2} = 131 \pm$

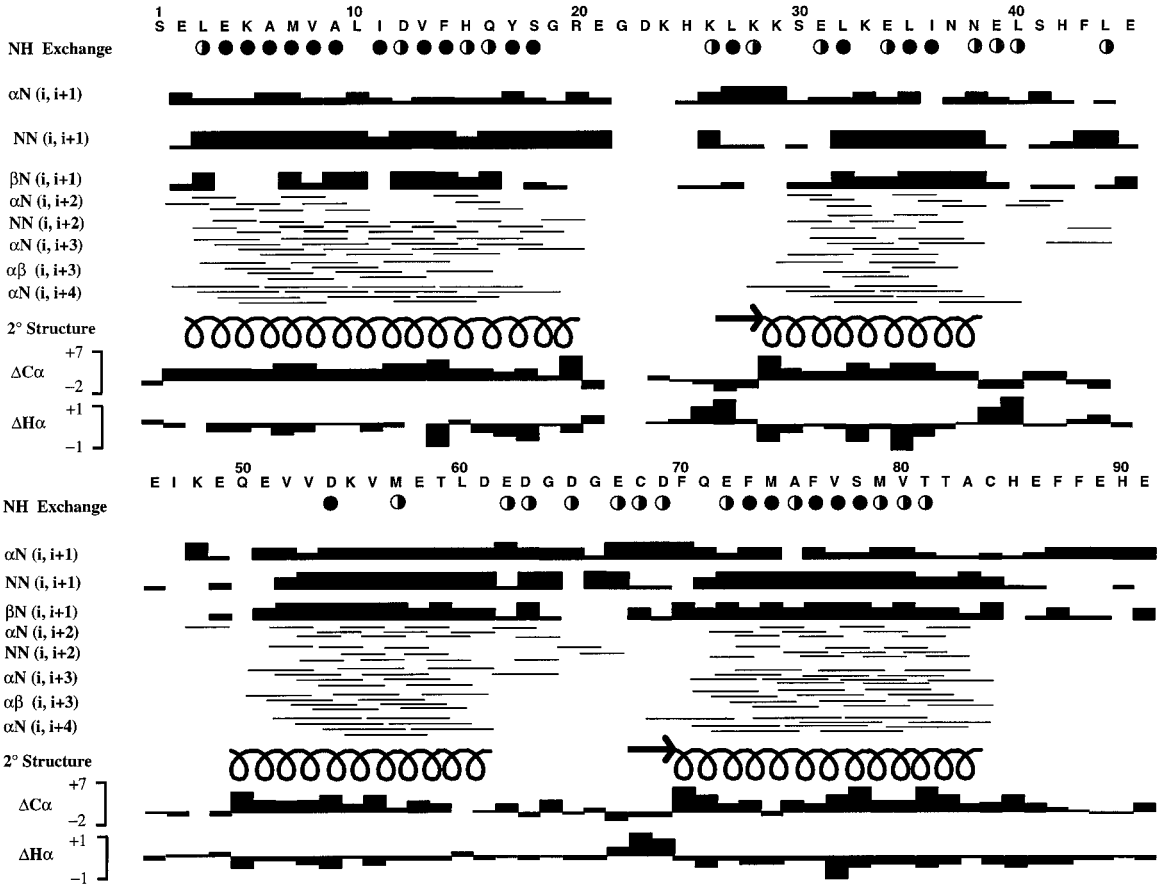

FIGURE 3: Diagram of NMR data used to determine the secondary structure of Ca^{2+}-bound S100B($\beta\beta$). Amide proton exchange rates are classified as slow (T > 18 h), medium (0.25 h < T < 18 h), and fast (T < 0.25 h) with solid, half-shaded, or no circle, respectively. Sequential and medium-range NOE and ROE correlations typical of elements of secondary structure are represented as previously described (*50*). Deviations in the $^{13}C_\alpha$ and $^1H_\alpha$ chemical shifts from those of a random coil are also shown (*81*, *82*). Together, these NMR data indicate that Ca^{2+}-bound S100B($\beta\beta$) has two β-strands (arrows) and four α-helixes (spirals).

5°, and $\Omega_{3-4} = 107 \pm 6°$) was similar to those found in several EF-hand-containing proteins, including Ca^{2+}-bound calbindin D_{9K}, troponin C, calmodulin, and parvalbumin (Ω_{3-4} ranges from 84 to 126°). Therefore, it was reasonable to position Ca^{2+} and its coordinating ligands in S100B($\beta\beta$) on the basis of data from high-resolution X-ray structures of Ca^{2+}-coordinated EF-hand proteins and on the basis of data from lanthanide luminescence studies of S100B($\beta\beta$).

Distance restraints (2.0−2.8 Å) in the typical EF-hand from Ca^{2+} to one carboxylate oxygen atom of D61, D63, and D65 (*X*, *Y*, and *Z* positions), to the carbonyl oxygen atom of E67 ($-Y$ position), and to both side chain oxygen atoms of E72 ($-Z$ and $-Z'$ positions) were based on the Ca^{2+} coordination model of Strynadka and James (*11*). Incorportion of these restraints was supported by lanthanide luminescence studies of the consensus EF-hand in S100B($\beta\beta$) which indicate that six coordination ligands are from the protein (*15*). The final ligand is likely provided by a water molecule at the $-X$ position (*11*, *66*) and was not included in the structure determination.

On the basis of the X-ray structure of the S100-hand in Ca^{2+}-bound calbindin D_{9K} (*62*), the carboxylate oxygen atoms of E31 in the pseudo EF-hand of S100β have been predicted to coordinate the $-Z$ and $-Z'$ positions of Ca^{2+} in a bidentate manner (*11*, *12*). Similarly, the remaining positions for Ca^{2+} coordination are thought to be filled by a single water molecule at the $-X$ position and by backbone carbonyl oxygen atoms from residues S18, E21, D23, and K26 at the *X*, *Y*, *Z*, $-Y$ liganding positions, respectively (*12*). However, studies using laser-induced lanthanide luminescence spectroscopy for this site indicate that only four of the seven ligands of Ca^{2+} are provided by S100β (*15*). Therefore, the structures of Ca^{2+}-bound S100B($\beta\beta$) determined without Ca^{2+} distance restraints were refined using all possible combinations of four residues liganded to Ca^{2+}. The ligands tested (given above) were analogous to the ligands in the S100-hand of Ca^{2+}-bound calbindin D_{9K} (*62*), plus the carboxylate oxygen atoms of E21 and D23. The carbonyl oxygens of S18 and K26, a side chain oxygen of E31, and the carbonyl oxygen of either E21 or D23 were found as probable ligands since no distance restraint violations of >0.5 Å were observed for this combination, whereas other schemes routinely violated distance restraints. Therefore, structure calculations which incorporated Ca^{2+} used distance restraints from Ca^{2+} to the carbonyl oxygens of S18 and K26, to a side chain oxygen of E31, and to the carbonyl oxygen of either E21 or D23.

The location of the Ca^{2+} ions within each S100β subunit (of structures calculated using the above coordination scheme) is reasonable since the distance between them of 14.1 ± 0.6 Å agrees with a distance of 15.0 ± 0.4 Å calculated from a Forster-type energy transfer between Eu^{3+} (donor) and Nd^{3+} (acceptor) bound in the normal and pseudo EF-hands, respectively (*15*). Furthermore, no dif-

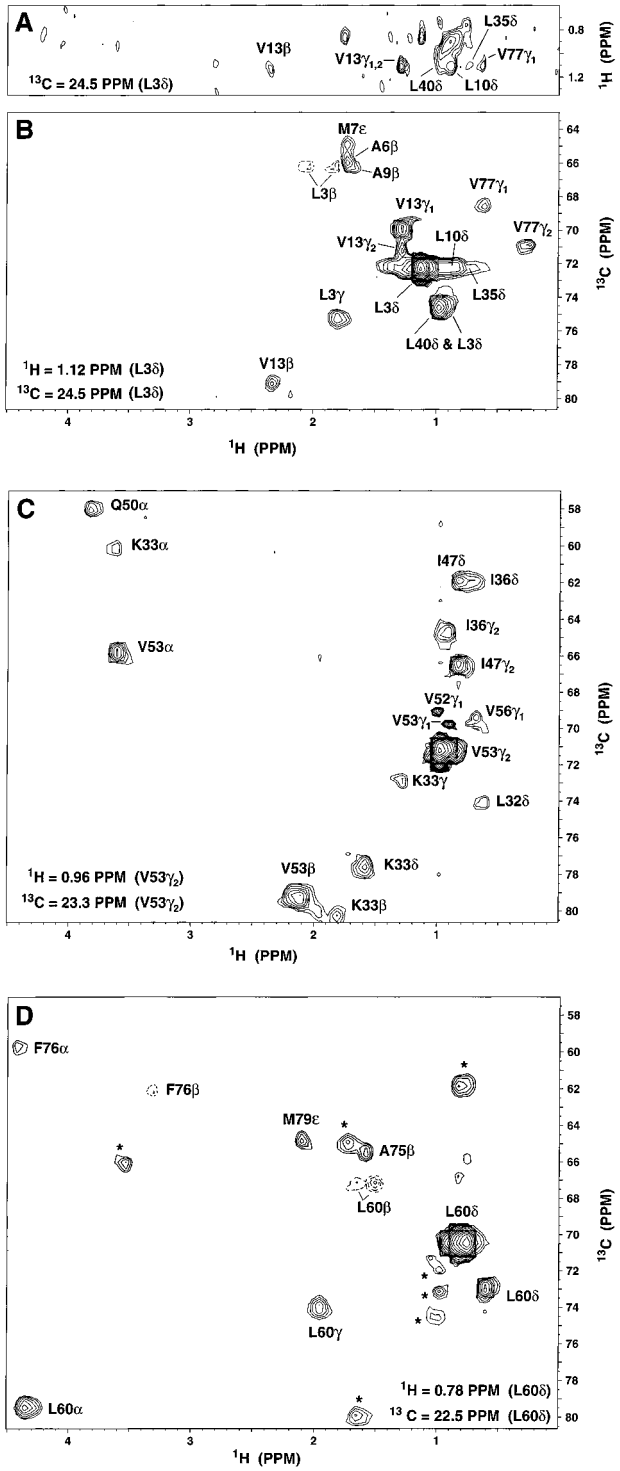

FIGURE 4: NOE spectra illustrating intermolecular NOE correlations at the dimer interface (A and B) and intramolecular NOE correlations to residues in helix 3 (C and D). (A) A strip from the 3D ^{13}C-edited, ^{12}C-filtered HMQC-NOESY spectrum showing intermolecular NOE correlations to L3H$_\delta$. (B) The corresponding plane from the 4D ^{13}C,^{13}C-edited NOESY spectrum shows both intra- and intermolecular NOE correlations to L3H$_\delta$. (C) A plane from the 4D ^{13}C,^{13}C-edited NOESY spectrum shows NOE correlations from V53H$_\gamma$ in helix 3 (N terminus) to residues in the hinge and helix 2. (D) A plane from the 4D ^{13}C,^{13}C-edited NOESY spectrum shows NOE correlations from L60H$_\delta$ in helix 3 (C terminus) to residues in helix 4. NOE correlations marked with asterisks maximize in neighboring planes.

ferences were observed for any interhelical angles when the protein structures determined with and without the Ca^{2+} restraints were compared (data not shown).

Structure of Ca^{2+}-Bound S100B($\beta\beta$). The structure of Ca^{2+}-bound S100B($\beta\beta$) was determined from 372 intraresidue, 556 sequential, 636 medium-range, 258 long-range, 138 intermolecular, 26 intra- and/or intermolecular, 152 hydrogen bond, and 20 Ca^{2+}−ligand distance restraints (11.9 distance restraints per residue) (Table 1; Figure 1, Supporting Information). Figure 5 illustrates a superposition (C_α) of the 20 final structures, none of which exhibited distance violations exceeding 0.5 Å or dihedral angle violations exceeding 5° (Table 1). The 20 structures are well converged with an rmsd from the mean structure of 1.27 ± 0.19 for backbone atoms in residues 1−88 and 1.92 ± 0.17 for all heavy atoms in residues 1−88, and low rmsds from the experimental restraints and idealized covalent geometry (Table 1). The rmsd between the two subunits is negligible as expected for a symmetric dimer. The 20 structures have an average of 87.7% residues in the most favorable region of the Ramachandran plot, and no structure has a residue in the disallowed region. The overall stereochemical quality of the 20 structures assessed by PROCHECK (*67*) indicates that the Ca^{2+}-bound S100B($\beta\beta$) structure corresponds to that of a 2 Å X-ray structure with an *R* factor of <20% (Table 1). The best of these structures (Figure 5) exhibits the lowest rmsds from the mean structure, the largest number of residues in the most favorable Ramachandran region (91.9%), and better than average values for nearly all other measures of quality from PROCHECK (Table 1).

Similarities between the Structures of Apo- and Ca^{2+}-Bound S100B($\beta\beta$). The secondary structure of each subunit (S100β) of Ca^{2+}-bound S100B($\beta\beta$) is consistent with the presence of two helix−loop−helix Ca^{2+} ion binding domains known as EF-hands (Figure 3). Each of the two Ca^{2+}-binding domains of an S100β subunit contains a short β-strand segment, K26−K28 (strand 1) and E67−D69 (strand 2), respectively, which align in an antiparallel manner (Figures 3 and 6) as found in rat apo-S100B($\beta\beta$) (*12*, *14*) and other EF-hand-containing proteins (*11*). In addition, the starting and ending points of the four helixes in each S100β subunit are similar to those found in the apoprotein (helix 1, E2−R20; helix 2, K29−N38; helix 3, Q50−D61; and helix 4, F70−A83).

The majority of hydrophobic residues observed at the dimer interface of apo-S100B($\beta\beta$) remain at the interface upon the addition of Ca^{2+}, including L3, A6, M7, V8, A9, L10, I11, V13, L35, L40, F43, F70, F73, M74, V77, V80, T81, T82, and F88. Indeed, F87 is the only residue for which intermolecular NOEs were observed in apo-S100B($\beta\beta$) but not in Ca^{2+}-bound S100B($\beta\beta$). An X-type four-helix bundle is observed at the dimer interface, as found in apo-S100B($\beta\beta$) (*14*), which is characterized by the nearly antiparallel alignment of helixes 1 and 1′ (−155 ± 4°) and of helixes 4 and 4′ (159 ± 5°) and the perpendicular association of these pairs of helixes (Figure 5 and Table 2). Intermolecular NOEs are observed in Ca^{2+}-bound S100B($\beta\beta$) from residues in helix 1 to residues of helix 2′ and loops 2′ and 4′ (the variable loops) of the other subunit. The large number of hydrophobic residues comprising the dimer interface, most of which are conserved in the S100 protein family, can easily explain the very high stability ($^{dimer}K_D$ < 500 pM) of this dimer motif in the apo or Ca^{2+}-bound state (*24*).

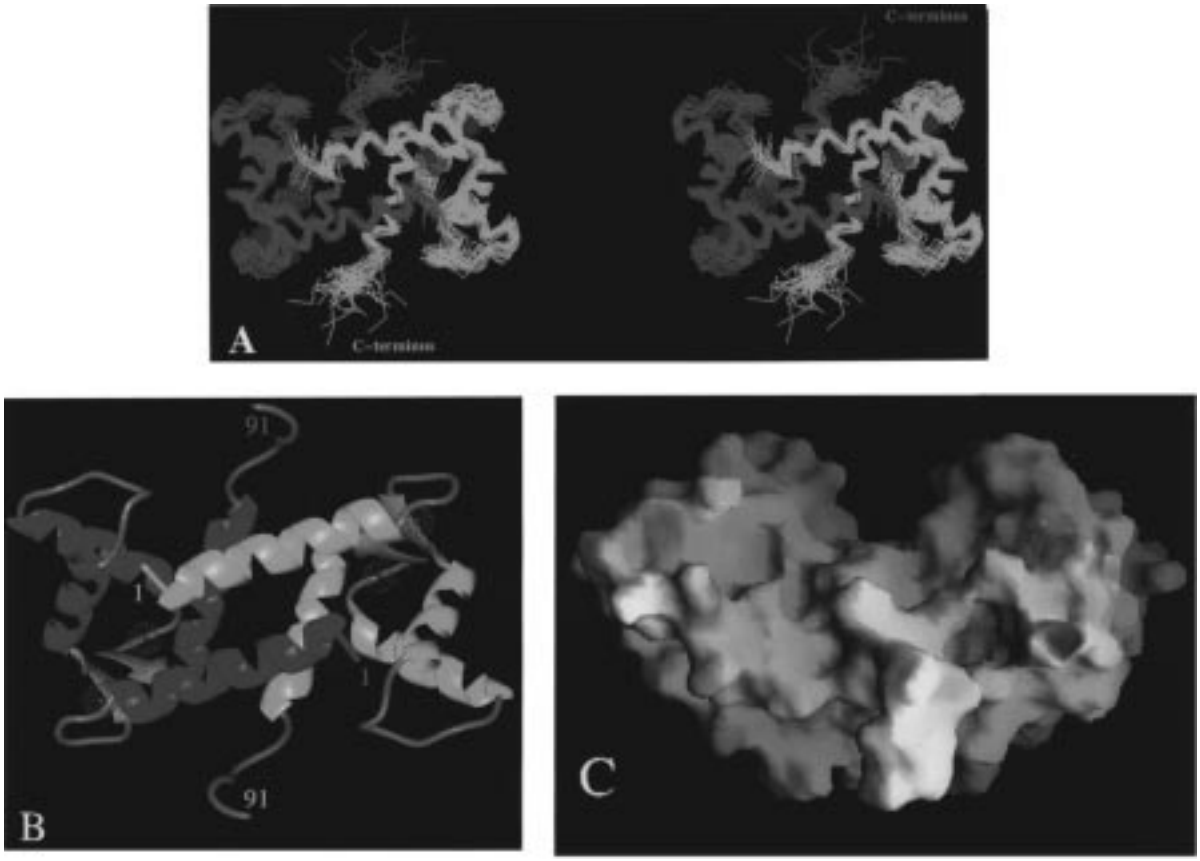

FIGURE 5: Structure of Ca^{2+}-bound S100B($\beta\beta$). (A) Stereoview of the 20 acceptable structures of Ca^{2+}-bound S100B($\beta\beta$) with the S100β subunits shown in yellow and cyan and Ca^{2+} ions shown in red. An α-carbon trace is shown for each structure, and they were aligned by Cα superposition. The statistical parameters for the structures are given in Table 1. Distance restraints involving Ca^{2+} were incorporated in the final stage of refinement as described in Materials and Methods. (B) Ribbon diagram of the best Ca^{2+}-bound S100B($\beta\beta$) structure (Table 1). (C) Molecular surface of Ca^{2+}-bound S100B($\beta\beta$) color coded by electrostatic potential. The orientation of the protein in this panel is identical with those in Figure 7.

Table 2: Interhelical Angles of EF-Hands in Ca^{2+}-Binding Proteins[a]

helixes	rat apo-S100B($\beta\beta$)[b,c]	apocalcyclin[d]	apocalbindin[e]	apocalmodulin[f]	Ca^{2+}−calmodulin[g]	Ca^{2+}−calbindin[h]	rat Ca^{2+}−S100B($\beta\beta$)[b,i]
1−2	$135 \pm 3^{\perp}$	$126 \pm 27^{\perp}$	$123 \pm 3^{\perp}$	$138 \pm 2^{\perp}$ (131 ± 4)$^{\perp}$	87 (105)$^{\perp}$	$128^{\perp}$	$137 \pm 5^{\perp}$
1−3	$-22 \pm 2^{\parallel}$	$-83 \pm 22^{\perp}$	$-109 \pm 9^{\perp}$	$-88 \pm 3^{\perp}$ (-81 ± 5)$^{\perp}$	160 (142)$^{\parallel}$	$-113^{\perp}$	$-118 \pm 5^{\perp}$
1−4	$121 \pm 2^{\perp}$	$119 \pm 17^{\perp}$	$128 \pm 4^{\perp}$	$127 \pm 2^{\perp}$ (142 ± 5)$^{\parallel}$	110 (119)$^{\perp}$	$120^{\perp,i}$	$128 \pm 4^{\perp}$
2−3	$-138 \pm 4^{\parallel}$	$144 \pm 15^{\parallel}$	$124 \pm 7^{\perp}$	$126 \pm 3^{\perp}$ (141 ± 5)$^{\parallel}$	113 (113)$^{\perp}$	$113^{\perp}$	$104 \pm 3^{\perp}$
2−4	$-36 \pm 2^{\parallel}$	$-16 \pm 10^{\parallel}$	$-34 \pm 4^{\parallel}$	$-47 \pm 2^{\perp}$ (-30 ± 5)$^{\parallel}$	-45 (-37)$^{\perp}$	$-28^{\parallel,i}$	$-35 \pm 4^{\parallel}$
3−4	$-140 \pm 2^{\parallel}$	$145 \pm 16^{\parallel}$	$118 \pm 8^{\perp}$	$130 \pm 3^{\perp}$ (133 ± 4)$^{\perp}$	84 (96)$^{\perp}$	$126^{\perp,i}$	$106 \pm 4^{\perp}$

[a] Interhelical angles (ϕ) range from −180 to 180° and are classified as either parallel (||) for $0° \leq |\Omega| \leq 40°$ and $140° \leq |\Omega| \leq 180°$ or perpendicular (⊥) for $40° < |\Omega| < 140°$ as described (*72*). The sign (+ or −) of Ω can be determined by (1) orienting the molecule so that the two helixes of interest (*i* and *j*) are in planes parallel to the screen with the first helix (*i*) in front of the second (*j*) and the first helix (*i*) aligned vertically (0°, with its N → C vector pointing upward), (2) aligning an imaginary vector vertically (0°) with its tail placed at the N terminus of the second helix (*j*), and (3) rotating the vector (by ≤180° clockwise or counterclockwise) to align with the N → C vector of the second helix (*j*) where a clockwise rotation gives a positive (+) Ω value and a counterclockwise rotation gives a negative (−) Ω value. [b] For S100B($\beta\beta$), Ω values were calculated using the program Iha 1.4. [c] Helixes in apo-S100β are as follows: helix 1, E2−S18; helix 2, K29−L40; helix 3, Q50−D62; and helix 4, F70−T82 (*14*). [d] Helixes in apocalcyclin are as follows: helix 1, 4−16; helix 2, 32−42; helix 3, 53−62; and helix 4, 70−85 (*68*). [e] Helixes in apocalbindin are as follows: helix 1, 3−13; helix 2, 25−35; helix 3, 46−54; and helix 4, 63−72 (*69*). [f] Helixes in apocalmodulin are as follows: helix 1, 6−18; helix 2, 29−38; helix 3, 45−54; and helix 4, 65−74 (*70*). Ω values for the third and fourth EF-hands in apocalmodulin are listed in parentheses next to the analogous helixes in the first and second EF-hands and are as follows: helix 5, 83−91; helix 6, 102−111; helix 7, 118−127; and helix 8, 139−145 (*70*). [g] Ω values from Babu et al. (*80*). [h] Ω values from Szebenyi et al. (*62*). Ω values from the center portion of the bent helix IV in calbindin as described in Szebenyi et al. (*62*). [i] Helixes in Ca^{2+}−S100β are as follows: helix 1, E2−R20; helix 2, K29−N38; helix 3, Q50−D61; and helix 4, F70−A83.

Although most residues of helix 1 participate in the dimer interface of Ca^{2+}-bound S100B($\beta\beta$), a large number of intramolecular interactions also contribute to its orientation. For example, C-terminal residues in helix 1 show NOEs to residues in the first Ca^{2+}-binding loop (loop 1) and helix 2 in the apo and Ca^{2+}-bound states. Accordingly, the interhelical angle of helixes 1 and 2 ($137 \pm 5°$) for Ca^{2+}-bound S100B($\beta\beta$) is the same as that of apo-S100B($\beta\beta$) ($135 \pm 3°$) and the pseudo EF-hands of other S100 proteins (Table 2) (*68*−*70*). Therefore, this pseudo EF-hand is poised to bind Ca^{2+} in the apo state as was observed for the pseudo hand of calbindin D_{9K} (*69*). The absence of a conformational

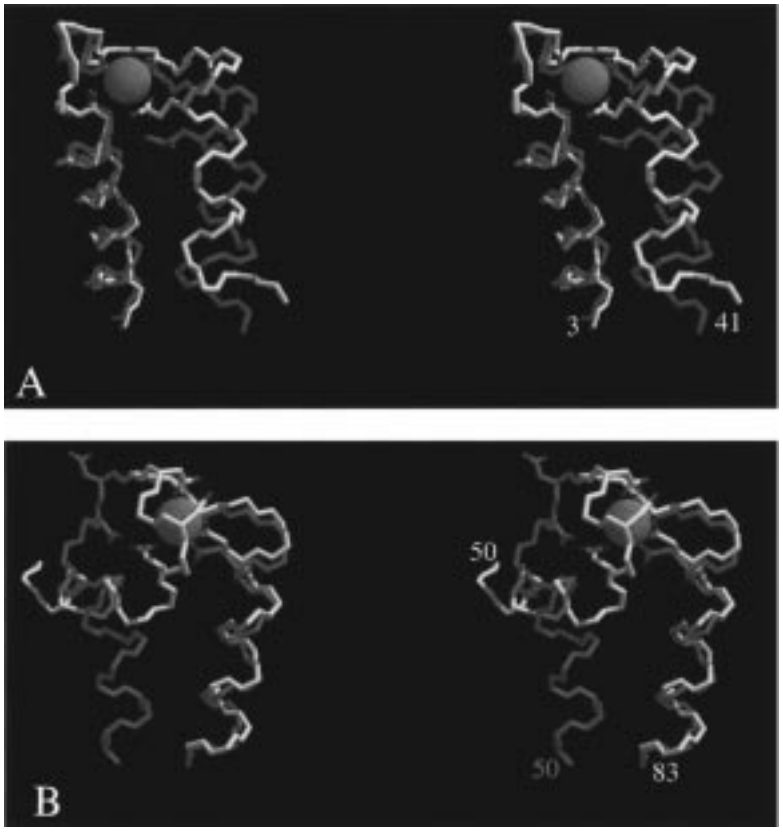

FIGURE 6: Comparison of the EF-hand Ca^{2+}-binding domains of apo- and Ca^{2+}-bound S100β subunits. (A) The pseudo EF-hand in apo- (blue) and Ca^{2+}-bound (white) S100β (residues L3−S41). The overlay was performed by matching backbone atoms in residues L3−L27. (B) The classical EF-hand in apo- (blue) and Ca^{2+}-bound (white) S100β (residues Q50−A83) (*14*). The overlay was performed by matching backbone atoms in residues E67−A83.

change in the pseudo EF-hand is not surprising since the orientation of helix 1 is restricted by the dimer interface in both Ca^{2+}-bound and apo-S100B($\beta\beta$) (*14*, *24*).

The Conformational Change. It has been known for many years that a conformational change occurs in S100B($\beta\beta$) when it binds Ca^{2+} (for reviews, see refs *2*−*5*). For the first time, the Ca^{2+}-dependent conformational change in S100B($\beta\beta$) can be described at the molecular level since 3D structures are now available for both the apo and Ca^{2+}-bound states. However, the extent of this conformational change is controversial since significant differences in the orientation of helix 3 (with respect to helixes 1, 2, and 4) are reported for various members of the S100 family in the apo state. These differences are well illustrated by the helix 3 to helix 4 interhelical angle (Ω_{3-4}): rat apo-S100B($\beta\beta$), $\Omega_{3-4} = -142 \pm 4°$ (*14*); bovine apo-S100B($\beta\beta$), $\Omega_{3-4} = 164 \pm 4°$ (*71*); apocalcyclin, $\Omega_{3-4} = 145 \pm 16°$ (*68*); and apocalbindin D_{9K}, $\Omega_{3-4} = 123 \pm 3°$ (*69*) (Table 2).

In this study, we compare the structure of rat Ca^{2+}-bound S100B($\beta\beta$) to rat apo-S100B($\beta\beta$) determined previously (*14*) for several reasons. First, the hinge region (loop 2) of S100B has three more residues than that of calbindin D_{9K} and calcyclin, which could have a significant effect on the orientation of helix 3. Another difference is that calbindin D_{9K} is a monomeric protein, whereas S100B and calcyclin are dimeric. Furthermore, the Ca^{2+}-bound and Ca^{2+}-free structures for rat S100B($\beta\beta$) are based on data from 2D, 3D, and 4D NMR. Therefore, both of these structures have a majority of their NOE correlations assigned unambiguously using chemical shift values alone. In addition, isotope-filtered NMR data using S100B($\beta\beta$) samples with asymmetrically labeled subunits were used in both of the rat structures in order to distinguish intra- from intermolecular NOE correlations (Figure 4A). Finally, the statistics in Table 1 for the structure of rat Ca^{2+}-bound S100B($\beta\beta$) are comparable to those of rat apo-S100B($\beta\beta$) (*14*) and make a comparison between these two structures most appropriate.

When the structures of S100B($\beta\beta$) from rats are compared, it is clear that helix 3 in the second EF-hand undergoes a very large change in orientation (>110°) upon the addition of Ca^{2+} (Table 2 and Figure 6). In Ca^{2+}-bound rat S100B($\beta\beta$), a large number of NOE correlations define the interaction of N-terminal residues of helix 3 with residues in helix 2. For example, unambiguous NOE correlations between residues V53 (N terminus of helix 3) and K29, K33, and I36 (in helix 2) are typical of those observed in this region (Figures 4C and 6). On the other hand, in apo-S100B($\beta\beta$), the N-terminal residues of helix 3 are found to interact with the C-terminal residues of helix 4 as defined by NOE correlations, including those from V52 and V53 (N terminus of helix 3) to M79, V80, and A83 (C terminus of helix 4). The helix 3 orientation in Ca^{2+}-bound S100B($\beta\beta$) is further defined by long-range NOEs from C-terminal residues of helix 3 to residues of helix 4, including unambiguous NOEs from L60 to A75, F76, and M79 (Figures 4D and 6) and from T59 to M79. On the other hand, the C terminus of helix 3 in apo-S100B($\beta\beta$) is in close proximity to the N terminus of helix 2 as defined by unambiguous NOE correlations from L60 to K29, L32, K33, and I36 (see Figure 4 of ref *14*). Unambiguous NOEs are also observed from

M57 of helix 3 to K29, L32, and K33 in the N terminus of helix 2 and K28, E67, and C68 in the β-sheet of Ca^{2+}-bound S100B($\beta\beta$). Whereas in apo-S100B($\beta\beta$), M57 exhibited unambiguous NOEs to I36 and N37 in the C terminus of helix 3, L44 in the hinge region, and V80 in the C terminus of helix 4. Accordingly, the four helixes of each S100β subunit resemble a splayed-type four-helix bundle (four perpendicular helixes). The splayed-type four-helix bundle was also observed in Ca^{2+}-bound calbindin D_{9K} (Table 2), whereas a unicornate-type (one helix perpendicular to three parallel helixes) was found in apo-S100B($\beta\beta$) (Table 2) (*14*, *72*). The significant conformational change observed upon Ca^{2+} addition readily explains the large differences we and Smith et al. observe in chemical shift values and amide exchange rates (*51*, *73*), and the many other Ca^{2+}-dependent effects observed previously (for reviews, see refs *2*−*5*).

The hinge region and the C-terminal loop in rat apo-S100B($\beta\beta$) form a surface encompassing the C-terminal regions of helixes 2 and 4 and the N-terminal region of helix 3 (*14*). Interestingly, the large change in the position of helix 3 upon the addition of Ca^{2+} causes significant changes in the structure and orientation of both the hinge region and the C-terminal loop. In the presence of Ca^{2+}, the N-terminal portion of the hinge region is proximal to the C-terminal loop and the C terminus of helix 4, whereas the C-terminal region of the hinge extends back toward the N-terminal region of helix 2 and away from helix 4 (Figure 5). The change in orientation of the hinge region, C-terminal loop, and helix 3 is likely responsible for the Ca^{2+} dependence observed in target protein binding.

Implications for Target Protein Binding. The hinge region and the C-terminal loop have the least amount of sequence in common with other S100 proteins, and are therefore suggested to interact directly with target proteins (*9*, *14*). For example, a peptide based on the hinge region of CP-10 was found to exhibit chemotactic activity similar to that of the full-length protein (*74*). Furthermore, mutation of residues in the C terminus of p11 was found to abolish annexin I binding (*75*). Chemical modification and mutagenesis of C84 in S100B($\beta\beta$) were found to decrease binding to τ-protein (*76*) and aldolase (*77*), respectively, and further indicate that the C terminus is an important region of S100B($\beta\beta$) for target protein binding. This cysteine residue (C84) is exposed in the structure of Ca^{2+}-bound S100B($\beta\beta$) as predicted from chemical modification studies (*19*).

S100B($\beta\beta$) has been shown to bind p53, inhibit its phosphorylation by PKC, and promote disassembly of the p53 tetramer in a Ca^{2+}-dependent manner (*18*). A peptide derived from the putative phosphorylation site and S100B binding domain of p53 was synthesized (residues 367−388) and used to study the Ca^{2+}-dependent interaction between S100B($\beta\beta$) and p53 (*78*, *79*). This domain is at the C terminus of p53 and is adjacent to the oligomerization domain. As observed for full-length p53 (*18*), the p53 peptide was found to be a good substrate for the catalytic domain of PKC, and its phosphorylation was inhibited by S100B($\beta\beta$) in a Ca^{2+}-dependent manner (*79*). Interestingly, the inhibition observed can be explained by the Ca^{2+}-dependent binding of S100B($\beta\beta$) to the p53 peptide substrate (*78*). The p53 peptide was found to bind dimeric S100B($\beta\beta$) with a stoichiometry of 2:1 at two identical sites on the symmetric dimer (*78*). Residues of Ca^{2+}-bound S100B($\beta\beta$) which show significant changes in their H_N and ^{15}N chemical shifts (>0.2 and >1.0 ppm, respectively) and have new NOE correlations upon the addition the p53 peptide are shown in Figure 7A. These residues are located in helix 1 (L3), the hinge region (S41, L44, E45, E46, and I47), helix 3 (V52, V53, V56, and T59), the second Ca^{2+}-binding loop (E62), helix 4 (S78, M79, and A83), and the C-terminal loop (C84−F88) (*78*). Interestingly, many of these residues define a cleft which is most likely the binding site for the p53 peptide (Figures 5C and 8A). This cleft does not exist in rat apo-S100B($\beta\beta$) (Figure 7B), since many of these residues (particularly those in helix 3) are buried in the hydrophobic core (*14*).

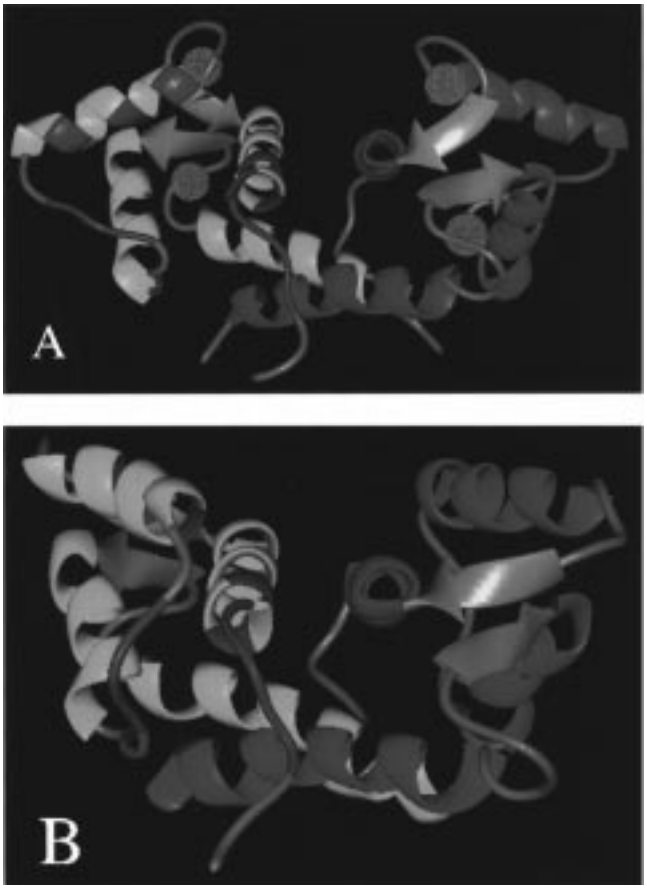

FIGURE 7: Comparison of the 3D structures of (A) Ca^{2+}-bound and (B) apo-S100B($\beta\beta$) from rats (*14*). Residues in one of the two symmetrical subunits of S100B($\beta\beta$) that change appreciably in chemical shift (H_N > 0.2 ppm, ^{15}N > 1.0 ppm) and exhibit new NOE correlations when the p53 peptide is titrated into Ca^{2+}-bound S100B($\beta\beta$) are shown in purple. While the same effects occur for residues in the other subuint, these residues are not highlighted in purple.

CONCLUSION

The three-dimensional structure of Ca^{2+}-bound rat S100B($\beta\beta$) has been determined using data from a series of 2D, 3D, and 4D NMR experiments. The S100β subunits contain four helixes and one antiparallel β-sheet, and they exhibit an X-type four-helix bundle at the symmetric dimer interface as found previously for rat apo-S100B($\beta\beta$) (*14*). However, a 112 ± 5° change of the interhelical angle between helixes 3 and 4 occurs in the normal EF-hand upon the addition of Ca^{2+}. This conformational change exposes a cleft defined

by residues in the hinge region, helix 3, and the C-terminal loop which is absent in the apo structure. This surface on Ca^{2+}-bound S100B($\beta\beta$) is likely important for target protein binding.

ACKNOWLEDGMENT

We are grateful to Dr. Marius Clore for providing source code and very helpful advice for implementing the conformational data base potential in X-PLOR, Dr. Stéphane Gagné for a program which calculates interhelical angles, and Dr. Peter Domaille for X-PLOR files.

SUPPORTING INFORMATION AVAILABLE

A table listing the NMR experiments (with the parameters) and a figure showing the number and distribution of NOE correlations by residue used in the structure determination of Ca^{2+}-bound S100B($\beta\beta$) (6 pages). Ordering information is given on any current masthead page.

REFERENCES

1. Moore, B. (1965) *Biochem. Biophys. Res. Commun. 19*, 739−744.
2. Kligman, D., and Hilt, D. (1988) *Trends Biochem. Sci. 13*, 437−443.
3. Donato, R. (1991) *Cell Calcium 12*, 713−726.
4. Zimmer, D. B., Cornwall, E. H., Landar, A., and Song, W. (1995) *Brain Res. Bull. 37*, 417−429.
5. Schafer, B. W., and Heizmann, C. W. (1996) *Trends Biochem. Sci. 21*, 134−140.
6. Allore, R., O'Hanlon, D., Price, R., Neilson, K., Willard, H. F., Cox, D. R., Marks, A., and Dunn, R. J. (1988) *Science 239*, 1311−1313.
7. Van Eldik, L. J., and Griffin, W. S. T. (1994) *Biochim. Biophys. Acta 1223*, 398−403.
8. Reeves, R. H., Yao, J., Crowley, M. R., Buck, S., Zhang, X., Yarowsky, P., Gearhart, J. D., and Hilt, D. C. (1994) *Proc. Natl. Acad. Sci. U.S.A. 91*, 5359−5363.
9. Kligman, D., and Marshak, D. R. (1985) *Proc. Natl. Acad. Sci. U.S.A. 82*, 7136−7139.
10. Kretsinger, R. H. (1980) *CRC Crit. Rev. Biochem. 8*, 119−174.
11. Strynadka, N. C. J., and James, M. N. G. (1989) *Annu. Rev. Biochem. 58*, 951−998.
12. Amburgey, J. C., Abildgaard, F., Starich, M. R., Shah, S., Hilt, D. C., and Weber, D. J. (1995) *J. Biomol. NMR 6*, 171−179.
13. Baudier, J., Glasser, N., and Gerard, D. (1986) *J. Biol. Chem. 261*, 8192−8203.
14. Drohat, A. C., Amburgey, J. C., Abildgaard, F., Starich, M. R., Baldisseri, D., and Weber, D. J. (1996) *Biochemistry 35*, 11577−11588.
15. Chaudhuri, D., Horrocks, W. W., Amburgey, J. C., and Weber, D. J. (1997) *Biochemistry 36*, 9674−9680.
16. Bianchi, R., Giambanco, I., and Donato, R. (1993) *J. Biol. Chem. 268*, 12669−12674.
17. Bianchi, R., Verzini, M., Garbuglia, M., Giambanco, I., and Donato, R. (1994) *Biochim. Biophys. Acta 1223*, 354−360.
18. Baudier, J., Delphin, C., Grundwald, D., Khochbin, S., and Lawrence, J. J. (1992) *Proc. Natl. Acad. Sci. U.S.A. 89*, 11627−11631.
19. Baudier, J., Mochly-Rosen, D., Newton, A., Lee, S.-H., Koshland, D. E., and Cole, R. D. (1987) *Biochemistry 26*, 2886−2893.
20. Lin, L.-H., Van Eldik, L. J., Osheroff, N., and Nordon, J. J. (1994) *Mol. Brain Res. 25*, 297−304.
21. Sheu, F.-S., Azmitia, E. C., Marshak, D. R., Parker, P. K., and Routtenberg, A. (1994) *Mol. Brain Res. 21*, 62−66.
22. Albert, K. A., Wu, W. C.-S., Nairn, A. C., and Greengard, P. (1984) *Proc. Natl. Acad. Sci. U.S.A. 81*, 3622−3625.
23. Wilder, P. T., and Weber, D. J. (1996) *Biophys. J. 70*, A62.
24. Drohat, A. C., Nenortas, E., Beckett, D., and Weber, D. J. (1997) *Protein Sci. 6*, 1577−1582.
25. Marion, D., Ikura, M., Tschudin, R., and Bax, A. (1989) *J. Magn. Reson. 85*, 393−399.
26. Bax, A., Ikura, M., Kay, L. E., and Zhu, G. (1991) *J. Magn. Reson. 91*, 174−178.
27. Delaglio, F., Grzesiek, S., Vuister, G. W., Zhu, G., Pfeifer, J., and Bax, A. (1995) *J. Biomol. NMR 6*, 277−293.
28. Zhu, G., and Bax, A. (1992) *J. Magn. Reson. 98*, 192−199.
29. Zhu, G., and Bax, A. (1990) *J. Magn. Reson. 90*, 405−410.
30. Live, D. H., Davis, D. G., Agosta, W. C., and Cowburn, D. (1984) *J. Am. Chem. Soc. 106*, 1939−1941.
31. Spera, S., and Bax, A. (1991) *J. Am. Chem. Soc. 113*, 5490−5492.
32. Edison, A. S., Abilgaard, F., Westler, W. M., Mooberry, E. S., and Markley, J. L. (1994) *Methods Enzymol. 239*, 3−79.
33. Jeener, J., Meier, B. H., Bachmann, P., and Ernst, R. R. (1979) *J. Chem. Phys. 71*, 4546−4553.
34. Kessler, H., Griesinger, C., Kerssebaum, R., Wagner, K., and Ernst, R. R. (1987) *J. Am. Chem. Soc. 109*, 607−609.
35. Bax, A., and Davis, D. G. (1985) *J. Magn. Reson. 65*, 355−360.
36. Mori, S., Abeygunawardana, C., Johnson, M. O., and Van Zijl, P. C. M. (1995) *J. Magn. Reson. 108*, 94−98.
37. Kay, L. E., Marion, D., and Bax, A. (1989) *J. Magn. Reson. 84*, 72−84.
38. Marion, D., Driscoll, P. C., Kay, C. M., Wingfield, P. T., Bax, A., Gronenborn, A. M., and Clore, G. M. (1989) *Biochemistry 28*, 6150−6156.
39. Ikura, M., Bax, A., Clore, G. M., and Groneborn, A. M. (1990) *J. Am. Chem. Soc. 112*, 9020−9022.
40. Vuister, G. W., and Bax, A. (1992) *J. Magn. Reson. 98*, 428−435.
41. Abeygunawardana, C., Weber, D. J., Gittis, A. G., Frick, D. N., Lin, J., Miller, A. F., Bessman, M. J., and Mildvan, A. S. (1995) *Biochemistry 34*, 14997−15005.
42. Muhandiram, D. R., Guang, Y. X., and Kay, L. E. (1993) *J. Biomol. NMR 3*, 463−470.
43. Wittekind, M., and Mueller, L. (1993) *J. Magn. Reson., Ser. B 101*, 205−210.
44. Grzesiek, S., and Bax, A. (1992) *J. Am. Chem. Soc. 114*, 6291−6293.
45. Vuister, G. W., Clore, G. M., Gronenborn, A. M., Powers, R., Garrett, D. S., Tschudin, R., and Bax, A. (1993) *J. Magn. Reson., Ser. B 101*, 210−213.
46. Muhandiram, D. R., Farrow, N. A., Xu, G.-Y., Smallcombe, S. H., and Kay, L. E. (1993) *J. Magn. Reson., Ser. B 102*, 317−321.
47. Starich, M. R. (1995) Ph.D. Thesis, University of Maryland Baltimore County, Baltimore, MD.
48. Bax, A., and Pochapsky, S. S. (1992) *J. Magn. Reson. 99*, 638−643.
49. Muhandiram, D. R., and Kay, L. E. (1994) *J. Magn. Reson., Ser. B 102*, 203−216.
50. Wuthrich, K. (1986) *NMR of Proteins and Nucleic Acids*, John Wiley, New York.
51. Smith, S. P., and Shaw, G. S. (1997) *J. Biomol. NMR 10*, 77−88.
52. Clore, G. M., Nilges, M., Sukumaran, D. K., Brunger, A. T., Karplus, M., and Gronenborn, A. M. (1986) *EMBO J. 5*, 2729−2735.
53. Nilges, M. (1993) *Proteins: Struct., Funct., Genet. 17*, 297−309.
54. Clore, G. M., Gronenborn, A. M., Nilges, M., and Ryan, C. A. (1987) *Biochemistry 26*, 8012−8013.
55. Brunger, A. T. (1992) *X-PLOR Version 3.1, A system for X-ray crystallography and NMR*, Yale University, New Haven, CT.
56. Nilges, M., Clore, G. M., and Gronenborn, A. M. (1988) *FEBS Lett. 229*, 317−324.
57. Nilges, M., Kuszewski, J., and Brunger, A. T. (1991) *Computational Aspects of the study of Biological Macromolecules by NMR*, Plenum Press, New York.
58. Kuszewski, J., Nilges, M., and Brunger, A. T. (1992) *J. Biomol. NMR 2*, 33−56.

59. Kuszewski, J., Qin, J., Gronenborn, A. M., and Clore, G. M. (1995) *J. Magn. Reson., Ser. B 106*, 92−96.
60. Kuszewski, J., Gronenborn, A. M., and Clore, G. M. (1996) *Protein Sci. 5*, 1067−1080.
61. Kuszewski, J., Gronenborn, A. M., and Clore, G. M. (1997) *J. Magn. Reson. 125*, 171−177.
62. Szebenyi, D. M. E., and Moffat, K. (1986) *J. Biol. Chem. 261*, 8761−8777.
63. Ferrin, T. E., Huang, C. C., Jarvis, L. E., and Langridge, R. (1988) *J. Mol. Graphics 6*, 13−27.
64. Nicholls, A., Sharp, K., and Honig, B. (1991) *Proteins: Struct., Funct., Genet. 11*, 281.
65. Smith, S. P., Barber, K. R., and Shaw, G. S. (1997) *Protein Sci. 6*, 1110−1113.
66. Denisov, V. P., and Halle, B. (1995) *J. Am. Chem. Soc. 117*, 8456−8465.
67. Laskowski, R. A., McArthur, M. W., Moss, D. S., and Thornton, J. M. (1993) *J. Appl. Crystallogr. 26*, 283−291.
68. Potts, B. C. M., Smith, J., Akke, M., Macke, T. J., Okazaki, K., Hidaka, H., Case, D. A., and Chazin, W. J. (1995) *Nat. Struct. Biol. 2*, 790−796.
69. Skelton, N. J., Forsen, S., and Chazin, W. J. (1990) *Biochemistry 29*, 5752−5761.
70. Kuboniwa, H., Tjandra, N., Grzesiek, S., Ren, H., Klee, C. B., and Bax, A. (1995) *Nat. Struct. Biol. 2*, 768−776.
71. Kilby, P. M., Van Eldik, L. J., and Roberts, G. C. K. (1996) *Structure 4*, 1041−1052.
72. Harris, N. L., Resnell, S. R., and Cohen, F. E. (1994) *J. Mol. Biol. 236*, 1356−1368.
73. Smith, S. P., Barber, K. R., Dunn, S. D., and Shaw, G. S. (1996) *Biochemistry 35*, 8805−8814.
74. Lackmann, M., Rajasekariah, P., Iismaa, S. E., Jones, G., Cornish, C. J., Hu, S., Simpson, R. J., Moritz, R. L., and Geczy, C. L. (1993) *J. Immunol. 150*, 2981−2991.
75. Kube, E., Becker, T., Weber, K., and Gerke, V. (1992) *J. Biol. Chem. 267*, 14175−14182.
76. Baudier, J., and Cole, R. D. (1988) *J. Biol. Chem. 263*, 5876−5883.
77. Landar, A., Hall, T. L., Cornwall, E. H., Correia, J. J., Drohat, A. C., Weber, D. J., and Zimmer, D. B. (1997) *Biochim. Biophys. Acta 1343*, 117−129.
78. Rustandi, R. R., Drohat, A. D., Baldisseri, D. M., Wilder, P. T., and Weber, D. J. (1998) *Biochemistry* (in press).
79. Wilder, P. T., Rustandi, R. R., Drohat, A. C., and Weber, D. J. (1998) *Protein Sci.* (in press).
80. Babu, Y. S., Bugg, C. E., and Cook, W. J. (1988) *J. Mol. Biol. 204*, 191−204.
81. Wishart, D. S., Sykes, B. D., and Richards, F. M. (1992) *Biochemistry 31*, 1647−1651.
82. Wishart, D. S., and Sykes, B. D. (1994) *J. Biomol. NMR 4*, 171−180.
83. Ferrin, T. E., Huang, C. C., Jarvis, L. E., and Langridge, R. (1988) *J. Mol. Graphics 6*, 36−37.

BI972635P